Hindawi
Advances in Multimedia
Volume 2022, Article ID 8940678, 10 pages
https://doi.org/10.1155/2022/8940678

Research Article

Engineering Safety Management System Based on Robot Intelligent Monitoring

Yanli Wang

Henan Technical College of Construction, Zhengzhou 450064, China

Correspondence should be addressed to Yanli Wang; wangyanlizd@163.com

Received 23 June 2022; Revised 11 July 2022; Accepted 27 July 2022; Published 21 August 2022

Academic Editor: Qiangyi Li

In order to improve the effect of engineering safety management, this paper combines intelligent monitoring technology to construct a monitoring robot system. Moreover, this paper analyzes the characteristics of the digital impulse signal and analyzes the least square filtering and infinite impulse response filtering. At the same time, this paper detects the sample material on the detection test platform, obtains the digital pulse signal, and selects different filtering algorithms and filtering parameters. In addition, this paper uses a signal analysis and processing platform to establish a gamma energy spectrum and analyze the resolution of hydrogen peaks in the gamma energy spectrum. Finally, this paper compares and verifies the filtering algorithms and constructs an engineering safety management system based on robot intelligent monitoring. From the simulation monitoring test results, it can be seen that the engineering safety management system based on robot intelligent detection proposed in this paper has a good effect.

1. Introduction

Driven by the rapid development of electronic technology, automation technology, computer, 5G, embedded technology, artificial intelligence, and other technologies, the Internet of Things technology is in a period of rapid development and is constantly penetrating into the field of building structural safety monitoring. For example, the application of sensing technology, data transmission technology, signal processing technology, and computer technology in construction projects has solved many difficult problems in traditional monitoring methods. How to perfectly combine the Internet of Things technology with traditional monitoring methods is an urgent issue that needs to be solved in the current development of building structural safety monitoring informatization. Therefore, with the help of the Internet of Things technology, the development of "Construction Engineering Monitoring and Supervision Early Warning Cloud Platform" has been developed to achieve real, timely, accurate, continuous, and quantifiable functions, easily understand the real-time deformation of buildings, standardize on-site operation behavior, automatically generate report information, monitor big data collation, and reduce the labor intensity of technicians, which has great social and economic value.

A relatively simple platform is built outside the single monitoring and supervision platform. The foundation pit monitoring database management system is established in the research, which mainly realizes the import function of foundation pit monitoring information, analyzes monitoring data in different formats, and determines the safety status of the foundation pit monitoring target [1]. The research introduces a Web-based foundation pit monitoring information management platform, which changes the traditional C/S architecture mode, can process monitoring data on the Web side, and realizes the sharing of monitoring data. The system is mainly used to manage monitoring data and draw images [2]. A deep foundation pit monitoring, forecasting, and alarming system has been established in the study, which mainly realizes the storage function of foundation pit monitoring data, uses the grey model to predict the database data, and uses several indicators to determine the safety status of the foundation pit project [3]. Using VisualBasic programming language and SQL database

management system, using visualization technology, on the basis of VB and GIS, developed a visualization analysis system for slope engineering monitoring information management [4]. The "Slope Monitoring Information Analysis System" has been developed, which can meet the functions of effective management of monitoring data, the visual query of monitoring data, analysis of slope stability according to monitoring data, and deformation prediction and early warning after analysis [5].

With the development of measurement technology, sensor, and automatic control technology, monitoring technology is also developing in the direction of automation and high-precision [6]. In the field of measurement and monitoring, if it is in an open area and the density of measuring points is not very large, static can already meet the requirements of deformation monitoring. For deep foundation pit construction monitoring, there are generally many monitoring points [7], and a new generation of the high-precision intelligent total station can be used to automatically monitor multiple measuring points at regular intervals to obtain real-time three-dimensional deformation data of the measuring points. In addition, the sensor manufacturing technology is also constantly developing, and the new generation of sensors will be more robust, reliable, stable, and high-precision [8]. Monitoring items such as groundwater level and soil stratified settlement test can also use automatic measurement and control instruments with corresponding sensor probes. Of course, the implementation of automatic monitoring technology is inseparable from automatic control technology, which requires a strong network communication system and control software as the backing, as well as excellent data analysis software that meets the needs of the site [9].

The monitoring content now includes the horizontal displacement of the top of the retaining wall, the vertical displacement of the top of the retaining wall, the horizontal displacement of the deep layer of the retaining wall, the internal force of the retaining wall, the internal force or deformation of the support, the displacement of the column, the tension of the anchor rod, the bottom of the pit Uplift, vertical displacement of soil layers, soil pressure before and after the retaining wall, pore water pressure, groundwater level, vertical displacement of the surface around the foundation pit, deformation of surrounding structures, and deformation of underground pipelines, etc. [10]. Analysis methods also proposed neural network forecasting method, real-time modeling time series analysis forecasting method, fuzzy mathematics forecasting method and grey system forecasting method, and other building foundation pit forecasting and forecasting methods [11].

In order to realize automatic monitoring and information management, researchers have developed various monitoring systems. For example, the engineering monitoring system constructed by *C*++, C#, and other languages can realize the management and analysis of monitoring data [12], so to a certain extent, the work intensity and difficulty of monitoring technicians are reduced. In addition, various online monitoring systems are more and more applied to foundation pit monitoring, such as foundation pit monitoring systems using ZigBee data transmission technology, automatic data collection using single chip technology and GPRS network, real-time monitoring systems using virtual instrument technology, the use of Web-based remote monitoring information management system, etc. [13]. In order to better display the monitoring data through images or graphics and realize the dynamic and intuitive display of the monitoring data, the visual 3D technology can be realized in the foundation pit monitoring, and the GIS technology is used to realize the 3D display of foundation pit monitoring information and data analysis and early warning function to achieve the purpose of information monitoring. As more and more attention is paid to informatization construction, BIM technology has also begun to be used in foundation pit monitoring. Combined with BIM technology, monitoring modules are added to the overall management of foundation pits during foundation pit construction, which improves the quality of engineering safety management and efficiency [14].

In terms of monitoring data processing research, simple mathematical statistical methods can no longer meet the needs of various data processing, and simply accepting monitoring data obviously cannot meet engineering needs. In order to achieve dynamic monitoring and management of projects, it is necessary to monitor objects and predict the changing trend. Since the monitoring data often contains various noise data, dead pixel data, and data interfered by other factors, these data often do not reflect the real state of the monitoring object, so the first thing to do when processing the monitoring data is to denoise and remove outliers. In addition, in order to realize the prediction of the changing trend, the researchers established various mathematical models to predict the changing trend. In order to improve the accuracy of forecasting, forecast and analyze data, combine a variety of single forecasting methods to form a combined model for data analysis, and use the advantages of various forecasting analysis methods to combine into a new data analysis model [15], for example, the combination of grey theory and artificial neural network for mathematical modeling and prediction [16]; the organic combination of multiple regression method and artificial neural network method can analyze the sequence of both linear trend and exponential growth trend [17]; in addition, many scholars have applied time series together with grey theory and established a combination model of grey-time series, in which the grey model is used to predict the changing trend of deformation, and the time series is used to predict the random part of deformation, etc. [18].

The significant advantages of automatic monitoring in observation frequency and accuracy can ensure the continuous and accurate monitoring requirements of the safety status of the gate station project and can record various monitoring data for a long time. Through data analysis and comparison, abnormal parameters that may lead to accidents can be found and alarmed in time. In the online analysis of engineering safety monitoring data, different alarm levels and corresponding upper and lower thresholds are usually set. When the online measurement data exceeds the set threshold range, the system will perform

corresponding alarm actions [19]. On the other hand, since all kinds of monitoring data are stored in the database for a long time, the system generally provides historical data query and data trend comparison interface or analysis tools [20], using offline query and analysis methods. For example, the least squares method or an improved method is used to model engineering safety monitoring data, eliminate outliers, and finally use it for data prediction.

This paper combines intelligent monitoring technology to construct a monitoring robot system to improve the effectiveness of project safety management and to provide a reference for follow-up project management.

2. Robot Monitoring Signal Processing

2.1. Pulse Signal Characteristic Analysis. After the characteristic gamma rays are collected by the crystal detector, converted and amplified by the photomultiplier tube, conditioned by the preprocessing circuit, collected by the high-speed acquisition card, and converted into analog-to-digital, the output is a digital pulse signal. Studying the characteristics of the spectrometer's digital pulse signal is the basis of studying the spectrometer's signal processing algorithm. The digital pulse signal has interference characteristics and peak shape characteristics.

The interference characteristics of digital pulse signals are mainly noise interference and overlapping pulse interference. Among them, noise interference occurs in all spectrometers, and overlapping pulse interference occurs in high count rate digitized spectrometers.

2.1.1. Noise Interference. Due to the interference of external factors in the process of signal acquisition, the system itself has errors in the process of data processing, and there is always noise in the digital pulse signal. Figure 1 shows a digital pulse signal, and the results of amplifying and observing some of the signals are shown in Figure 2.

It can be observed from Figure 2 that the noise in this segment of the digital pulse signal appears as irregular fluctuations at the baseline, and there are burrs on the pulse peak. The fluctuation of the baseline and the burr phenomenon on the pulse peak will cause problems such as difficulty in distinguishing between true and false peaks, and difficulty in determining the true position of the pulse peak, thus greatly reducing the resolution of the spectrometer.

The use of pulse signal digital filtering technology can stabilize the baseline, suppress pulse signal burr noise, and improve the resolution of the spectrometer. Therefore, before converting the digital pulse signal into a gamma energy spectrum, the pulse signal needs to be smoothed and filtered.

2.1.2. Overlapping Peak Characteristics. A set of overlapping pulses is shown in Figure 3. The pulse peak whose peak address is around 20 is peak 1, and the pulse peak whose peak address is around 50 is peak 2. It can be found that the falling edge of peak 1 and the rising and falling edge of peak 2 overlap, therefore, the data of each point where the falling edge of peak I and the rising edge of peak 2 overlap.

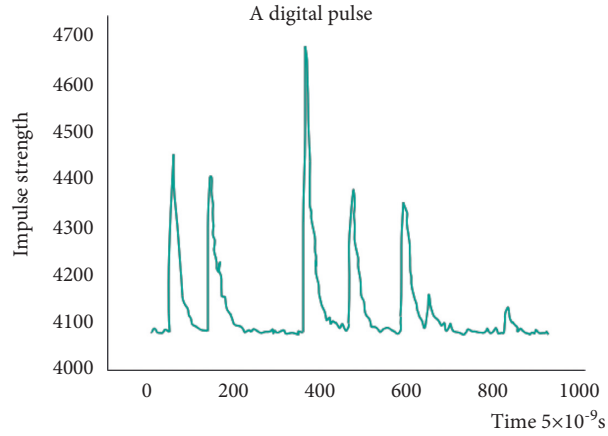

Figure 1: A digital pulse signal.

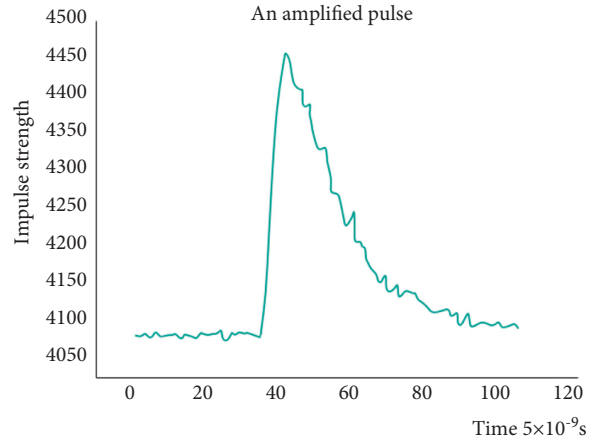

Figure 2: The enlarged part of the pulse signal.

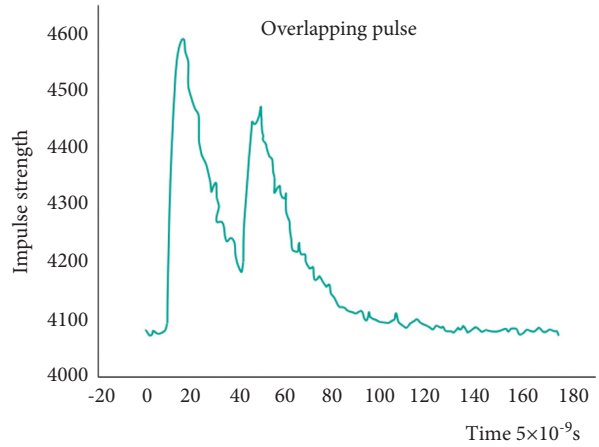

Figure 3: Overlapping pulses.

However, it is not actually the data read in the figure. That is, it cannot be obtained directly. We need to obtain the peak height data of peak 1 and peak 2. Due to the characteristics of peak shape, this overlapping phenomenon has no effect on the detection of the peak height of peak 1. However, the peak height of peak 2 in the figure is not the actual peak height,

and the peak height read by peak 2 is larger than its actual peak height. This peak height error will affect the resolution of the spectrometer.

Due to the existence of the pulse overlapping phenomenon, the pulse overlapping peaks need to be processed in the process of converting the pulse data into the gamma energy spectrum.

2.2. Digital Pulse Signal Peak Shape Characteristics. By observing the pulse data in Figures 1 to 3, it can be seen that the pulse peak shape has the following characteristics:

(1) The rising edge width of the digital pulse signal of the spectrometer is narrow, and the rising speed is fast. The falling edge is wider, the falling speed is slower, and the boundary with the baseline is not clear.

(2) For digital pulses with different peak heights, the pulse width, rising edge width, and falling edge width are all approximately equal.

According to the above two digital pulse peak shape characteristics, in the process of digital pulse signal peak searching and overlapping peak processing, it can be considered that the pulse width, the rising edge width, and the falling edge width are correspondingly equal, which simplifies the processing process. When the pulses overlap, it can be considered that the peak height of the pulses whose falling edges overlap is not affected.

It can be seen from the interference characteristics of the pulse signal that there is a lot of burr noise interference in the pulse signal, and smooth filtering is required before the pulse signal is converted into a gamma energy spectrum. Regarding the smoothing and filtering of signals, the following methods are commonly used.

2.2.1. Mean Filter. Mean filtering is a filtering algorithm with a relatively simple principle, and its feasibility is strong. It is a linear filtering technology. It uses the average value of the data of the point to be filtered and the data of each point in its neighborhood as the filtered value of the point to be filtered, which can be expressed by the formula:

$$\overline{S}(x) = \frac{1}{N} \times \sum_{k=i}^{j} S(k). \tag{1}$$

Among them, $\overline{S}(x)$ represents the filtered value of a point, S (k) represents the value of each point in the neighborhood of the point, and N represents the number of points in the neighborhood.

Mean filtering simply uses the average value in a neighborhood to represent the value of the middle point of the neighborhood. Although the method is relatively simple, it ignores the proportion of the influence of each point in the neighborhood on the center point. Moreover, the mean filter is suitable for suppressing periodic noise interference, but it has a poor ability to suppress high-frequency noise of digital pulse signals.

2.2.2. Gaussian Filter. Gaussian filtering is a linear smoothing filter. In fact, it is a special weighted moving average filter, and the Gaussian function is its weight. The Gaussian function is shown in the formula:

$$g(x) = \frac{1}{\sqrt{2\pi}\sigma} \exp\left(\frac{-x^2}{2\sigma^2}\right). \tag{2}$$

Among them, σ represents the distribution parameter of the Gaussian function, which directly determines the function value. Therefore, using the Gaussian function value as the weight for moving average filtering has the following characteristics:

(1) Since the Gaussian function is centrally symmetric, the weights are symmetric around the point to be filtered.

(2) The distribution range and size of the Gaussian function weight are determined by the distribution parameter σ. The smaller the σ is, the smaller the Gaussian distribution range and the less obvious the smoothing effect. The larger the σ, the larger the Gaussian distribution range and the more obvious the smoothing effect.

Gaussian filtering mainly suppresses Gaussian noise, and the noise in digital pulse signal is not Gaussian noise, so Gaussian filtering is not suitable for digital pulse signal filtering.

2.2.3. Wavelet Transform Filtering. Wavelet transform filtering is a hot research topic in recent years. It decomposes the data to be filtered and filters out noise interference.

For a function $F(u) \in L^2(R)$, its wavelet transform can be defined as follows:

$$W_F(s,u) = \frac{1}{s} \int F(t)\varphi\left(\frac{u-t}{s}\right)dt = \int \varphi_s(u-t)F(t)dt. \tag{3}$$

Among them, $\varphi_s(u-t)$ represents the scaling transformation of the mother wavelet $\varphi(u)$, s is the size scaling parameter, and t is the translation parameter.

Through wavelet transform, the effective part of the signal and the noise part are separated on the spectrum, so as to achieve the purpose of extracting and deleting the noise part. The recovery conditions of wavelet transform are as follows:

$$\int_0^{+\infty} \frac{|\widehat{\varphi}(\alpha)|^2}{\alpha} d\alpha = \int_{-\infty}^{0} \frac{|\widehat{\varphi}(\alpha)|^2}{\alpha} d\alpha = C_\varphi < +\infty. \tag{4}$$

When formula (4) is satisfied, the expression for restoring the original signal after wavelet transform can be written:

$$F(u) = \frac{1}{C_\varphi} \int_0^{+\infty} \int_{-\infty}^{+\infty} W_F(s,t)\overline{\varphi}_s(t-u)\frac{dsdt}{s}. \tag{5}$$

Wavelet change filtering is theoretically strong, but the filtering process is more complicated, and it is not suitable

for the processing of large data volume of spectrometer signals.

2.2.4. Kalman Filter. Kalman filtering is widely used. It mainly uses the linear state equation to optimally estimate the data according to the input and output of the system. The optimal estimation process is actually filtering.

The Kalman filter describes the system with a linear differential equation:

$$X(k) = AX(k-1) + BU(k) + \omega(k). \tag{6}$$

Equation (6) represents the process of deriving the current state $X(k)$ from the previous state $X(k-1)$. Among them, A and B are transfer parameters, and $U(k)$ is the control amount at time k. If there is no control quantity, $U(k)$ is 0, and $o(k)$ represents the noise of the transfer process. The state observation value at time k can also be obtained by the formula:

$$Z(k) = HX(k) + \delta(k). \tag{7}$$

Formula (7) is the observation function, $Z(k)$ represents the measured value at time k, H represents the transfer function from the actual value to the observed value during the measurement process, and $\delta(k)$ represents the observation error.

Due to the existence of the system transmission error $\omega(k)$ and the observation error $\delta(k)$, neither the current state $X(k|k-1)$ nor the measured value $Z(k)$ derived from the state at time $k-1$ is the actual value. Kalman filtering is to estimate the actual state at the current moment for the above two quantities.

Kalman filtering is suitable for real-time optimal estimation of data, but it is too complicated to apply it to digital signal filtering.

2.3. Research on Digital Filtering Algorithm of Pulse Signal. Least squares filtering is a method that can be used for smoothing filtering of pulsed signals. The main principle of this method is to take K points on the left and right of the point p to be filtered and perform least squares fitting on these $2K+1$ points. The value of point p on the fitted curve is the value of point p after smoothing.

If the prefiltering pulse value is S_i and the postfiltering pulse value is $\overline{S}_i$, then the prefiltering pulse value at point p is S_p, and the postfiltering pulse value is $\overline{S}_p$. The m-th order polynomial fit to $2K+1$ points is shown in the formula:

$$\begin{aligned} Y(x) = a_0 + a_1(x-p) + a_2(x-p)^2 \\ + a_3(x-p)^3 + \ldots + a_m(x-p)^m. \end{aligned} \tag{8}$$

Therefore, the filtered value of point p is as follows:

$$\overline{S}_p = Y(x)|_{x=p} = a_0. \tag{9}$$

Least square filtering needs to minimize the squared difference before and after filtering, that is, to find the solution that minimizes the formula:

$$\sum_{i=1}^{a} (S_i - \overline{S}_i)^2. \tag{10}$$

We can solve the following results:

$$\overline{S}_i = \sum_{j=k}^{k} f_{n,j} S_{i+j}. \tag{11}$$

Among them, $f_{n,j}$ is the coefficient of each item, $n = 2K+1$. $f_{n,j}$ can be obtained by the following formula:

$$f_{n,j} = \frac{1}{n}\left[1 + \frac{15}{n^2-4}\left(\frac{n^2-1}{12} - j^2\right)\right], \tag{12}$$

$$f_{n,j} = \frac{1}{n}\left[1 + \frac{105}{4\left(n^2-4\right)\left(n^2-16\right)}\left[\frac{5}{2}\left(n^2-7\right)\left(\frac{n^2-1}{12} - j^2\right) - 9\left(\frac{\left(n^2-1\right)\left(3n^2-7\right)}{240}\right) - j^4\right]\right], \tag{13}$$

$$f_{n,j} = \frac{1}{n}\left[1 + \frac{15\left(3n^2-7\right)}{\left(n^2-4\right)\left[\left(n^2-5\right)+4\right]}\left[\left(\frac{\left(n^2-1\right)\left(3n^2-7\right)}{240}\right) - j^4\right]\right]. \tag{14}$$

When using quadratic and cubic polynomials for fitting, the coefficients are calculated using formula (12). When fitting with a quartic or quintic polynomial, the coefficients are calculated using formula (13). When fitting with a box filter, the coefficients are calculated using formula (14). The coefficients are usually tabulated for convenience. The common calculation formula, such as the five-point cubic polynomial least squares fitting filter, is as follows:

$$\overline{S}_p = \frac{1}{35}\left(-3S_{p-2} + 12S_{p-1} + 17S_p + 12S_{p+1} - 3S_{p+2}\right). \tag{15}$$

By choosing the appropriate fitting order and number of points, the least square filtering can be used to suppress the noise in the digital pulse signal.

Usually, the design of a digital filter is to design the system transfer function. The transfer function of a filter system is as follows:

$$H(z)_{z=e^{j\omega}} = H\left(e^{j\omega}\right) = \sum_{n=0}^{\infty} h(n)e^{j\omega n},$$

$$H\left(e^{j\omega}\right) = |H(\omega)|e^{j\varphi(\omega)},$$

$$|H(\omega)| = \sqrt{\mathrm{Re}^2\left[H\left(e^{j\omega}\right)\right] + \mathrm{Im}^2\left[H\left(e^{j\omega}\right)\right]}, \quad (16)$$

$$\varphi(\omega) = arctg\frac{\mathrm{Im}\left[H\left(e^{j\omega}\right)\right]}{Rc\left[H\left(e^{j\omega}\right)\right]},$$

$$\omega = \Omega T = \Omega / f_s.$$

In the above five equations, $H(e^{j\omega})$ is the transfer function of the filter system, $h(n)$ is the unit impulse response of the filter, $H(\omega)$ is the amplitude response characteristic, $\varphi(\omega)$ is the phase response characteristic, Ω is the analog angular frequency, T is the sampling time interval, and f_s is the sampling frequency.

Since the noise signal is a high-frequency signal in the digital pulse signal, the designed low-pass filter has the following ideal characteristics:

tIn Figure 4, the black part represents the low frequency passband, and the rest represents the high-frequency stopband. However, the amplitude-frequency characteristics of the actual low-pass filter are not so ideal, as shown in Figure 5.

Among them, ω_p is the passband cut-off frequency, ω_s is the stopband cut-off frequency, the frequency $0 \sim \omega_p$ is the low frequency passband, the frequency $\omega_p \sim \omega_s$ is the transition band, and the frequency d is the high-frequency stopband.

The infinite impulse response low-pass filter is a type of low-pass filter that conforms to the characteristics of Figure 5. The design process is as follows:

(1) The algorithm gives filter parameters, such as passband cut-off frequency ω_p, stopband cut-off frequency ω_s, 3 dB cut-off frequency Ω_c, maximum attenuation A in the passband, minimum attenuation A in the stopband, etc.

(2) The algorithm designs an analog filter that meets the index according to the given parameters.

(3) The algorithm converts the analog filter to a digital filter.

(4) The algorithm designs the filter program according to the digital filter system function expression. The conversion methods from analog filters to digital filters are as follows:

2.3.1. Impulse Response Invariant Method. The unit impulse response of the digital filter is $h(n)$, and the unit impulse response of the analog filter is $h_a(nT)$.

$$h(n) = h_a(t) = h_a(nT). \quad (17)$$

The Z transform of $h(n)$ is $H(z)$, and the Laplace transform of $h_a(t)$ is $H_a(s)$. Then, according to formula (17), we can get the following:

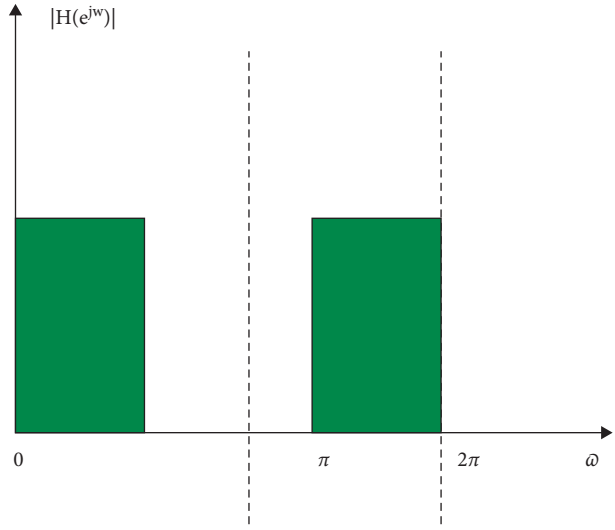

Figure 4: Ideal characteristics of a low-pass filter.

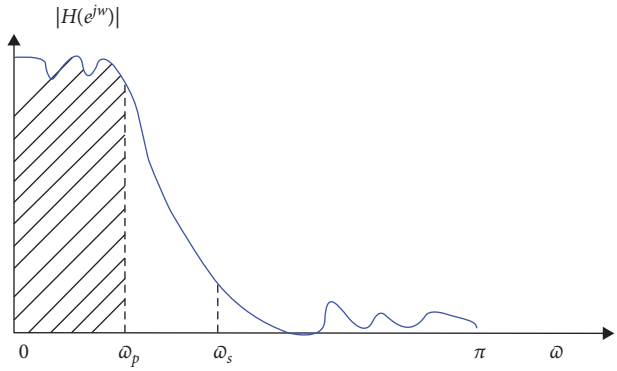

Figure 5: Actual characteristics of low-pass filter.

$$H(z)_{z=e^{j\omega}} = \frac{1}{T}\sum_{m=-\infty}^{\infty} H_a\left(j\frac{\omega + 2\pi m}{T}\right). \quad (18)$$

According to formula (18), the analog filter transfer function can be converted into a digital filter. Impulse-response-invariant method will cause the interference phenomenon of spectral overlap.

2.3.2. Bilinear Transformation Method. The bilinear transformation method is to compare the S plane first and then transform it to the Z plane. Therefore, the bilinear transform method does not produce spectral overlap, but high-frequency signals are easily distorted.

The transfer function of the analog filter is $H(s)$. According to the bilinear transformation method, the transfer function of the digital filter is as follows:

$$H(z) = H(s)|s = \frac{1 - z^{-1}}{1 + z^{-1}} = H\left(\frac{1 - z^{-1}}{1 + z^{-1}}\right). \quad (19)$$

After conversion by the impulse response invariant method or the bilinear transformation method, the system

function expression of the infinite impulse response low-pass filter is as follows:

$$H(z) = \frac{Y(z)}{X(z)} = \frac{\sum_{k=0}^{N} a_k z^{-k}}{1 + \sum_{k=1}^{N} b_k z^{-k}}, \tag{20}$$

where b_k is not all zero. That is, there is feedback in the system loop. Otherwise, it is a finite impulse response filter (FIR filter).

By expanding (20) and performing the inverse transformation of the Z change, the structural expression of the infinite impulse response low-pass filter can be obtained:

$$Y(n) = \sum_{k=0}^{N} a_k X(n-k) - \sum_{k=1}^{N} b_k Y(n-k). \tag{21}$$

In the formula, a_k and b_k are the low-pass filter coefficients, respectively, $X(n)$ is the value before filtering, $Y(n)$ is the value after filtering, and N is the filter order.

From formula (21), the following filter structure expression can be obtained:

$$Y(n) = a_0 X(n) + a_1 X(n-1) - b_1 Y(n-1), \tag{22}$$

$$\begin{aligned} Y(n) = {} & a_0 X(n) + a_1 X(n-1) + a_2 X(n-2) \\ & - b_1 Y(n-1) - b_2 Y(n-2), \end{aligned} \tag{23}$$

$$\begin{aligned} Y(n) = {} & a_0 X(n) + a_1 X(n-1) + a_2 X(n-2) \\ & + a_3 X(n-3) - b_1 Y(n-1) \\ & - b_2 Y(n-2) - b_3 Y(n-3). \end{aligned} \tag{24}$$

Formulas (22)–(24) are the expressions of the first-order, second-order, and third-order infinite impulse response low-pass filters, respectively. By using Matlab software to write a filter program and input parameters such as cut-off frequency, the low-pass filter coefficients a_{k} and b_{k} can be obtained.

Common infinite impulse response low-pass filters include Butterworth low-pass filters, Chebyshev low-pass filters, and elliptic filters.

The characteristics of the Butterworth low-pass filter are that the passband and stopband have no fluctuation, monotonically decrease, and the transition band decays slowly, and its characteristics are shown in Figure 6(a).

Chebyshev low-pass filters are proposed based on Chebyshev distribution, including Chebyshev type I and Chebyshev type II. The Chebyshev type I low-pass filter has ripples in the passband and no ripples in the stopband. However, the Chebyshev II low-pass filter has no ripple in the passband and ripple in the stopband. The attenuation bandwidth of the two Chebyshev low-pass filters is the same, and the attenuation is faster than the Butterworth low-pass filter. The characteristics of the two Chebyshev low-pass filters are shown in Figures 6(b) and 6(c).

The elliptic filter is also called the Cauer filter, and its passband and stopband fluctuate, and the attenuation speed of the attenuation band is faster than that of the Chebyshev low-pass filter, which is the fastest among the above filters. Its characteristics are shown in Figure 6(d).

For an infinite impulse response filter, its filtering order affects the filtering result. In theory, the higher the order, the better the filtering effect, but it will also increase the complexity of the filtering system, which needs to be considered dialectically. Using the Butterworth filter, Chebyshev filter and ellipse filter functions in Matlab software, the filter program can be designed to obtain the filter coefficients a_k and b_k. The design methods of infinite impulse response filter in Matlab include the impulse response invariant method and bilinear transformation method. Among them, the impulse response invariant method is prone to spectral aliasing, and the bilinear transform method is easy to distort at high frequencies. Since the purpose of digital pulse filtering is to filter high-frequency noise, the bilinear transform method can be considered.

3. Engineering Safety Management System Based on Robot Intelligent Monitoring

The monitoring system is divided into a preparation stage, a data acquisition module, a data communication module, a data processing module, and a data analysis and early warning module. Its logical structure is shown in Figure 7. The data preparation stage mainly involves the in-depth understanding of the specific monitoring method design, specification requirements, and technical parameters of the monitoring project. The data acquisition module mainly collects data from reference points and monitoring points or grid points planned in advance through the monitoring system to realize automatic and intelligent monitoring. The data communication module mainly completes the transmission of monitoring data according to the communication link described above and realizes the purpose of remote data transmission. The data processing module mainly stores, manages, and analyzes the monitoring data through the computer. The data analysis module is mainly used to predict and analyze the data in the database and calculate the relative displacement change of two periods and the cumulative displacement. When these calculation results exceed the specified limit of the project, the administrator will be alerted by e-mail or short message according to the number of overlimit points.

The intelligent automatic target search and recognition (ATR) function is the key technology for the measurement robot to realize automatic measurement. It separates the ATR beam reflected from the prism from the visible light and ranging beam through a special beam splitter in the telescope and guides the ATR beam to the CCD array inside the instrument to form an image and analyze it. After that, it calculates the prism center by the image processing method. Then, after obtaining the center position of the prism, the measuring robot controls the servo motor to precisely move the telescope to gradually align the center of the prism by calculating the offset between the center of the prism and the center of sighting. The workflow chart is shown in Figure 8.

The performance of the robot in engineering safety error monitoring is studied through the simulation platform, and

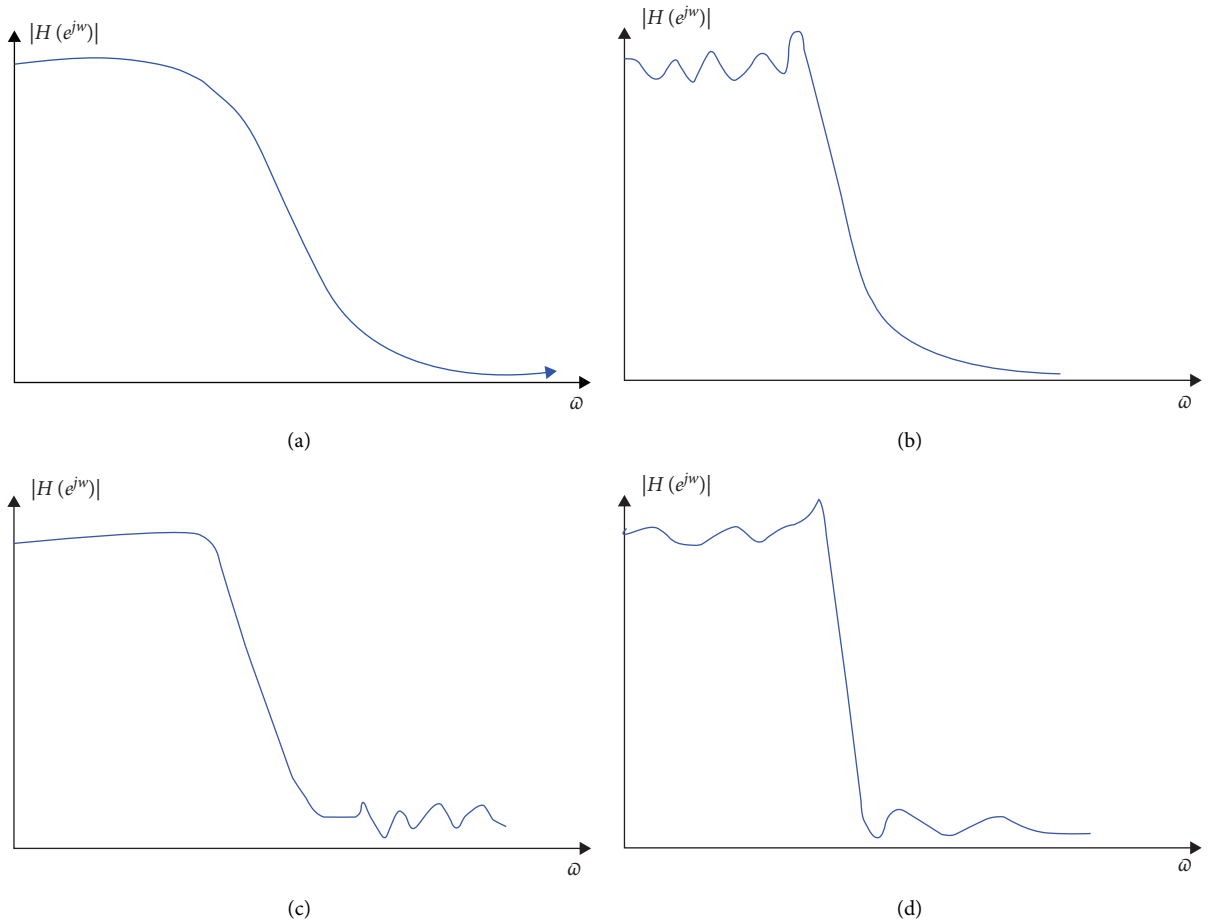

Figure 6: Characteristics of several filters.

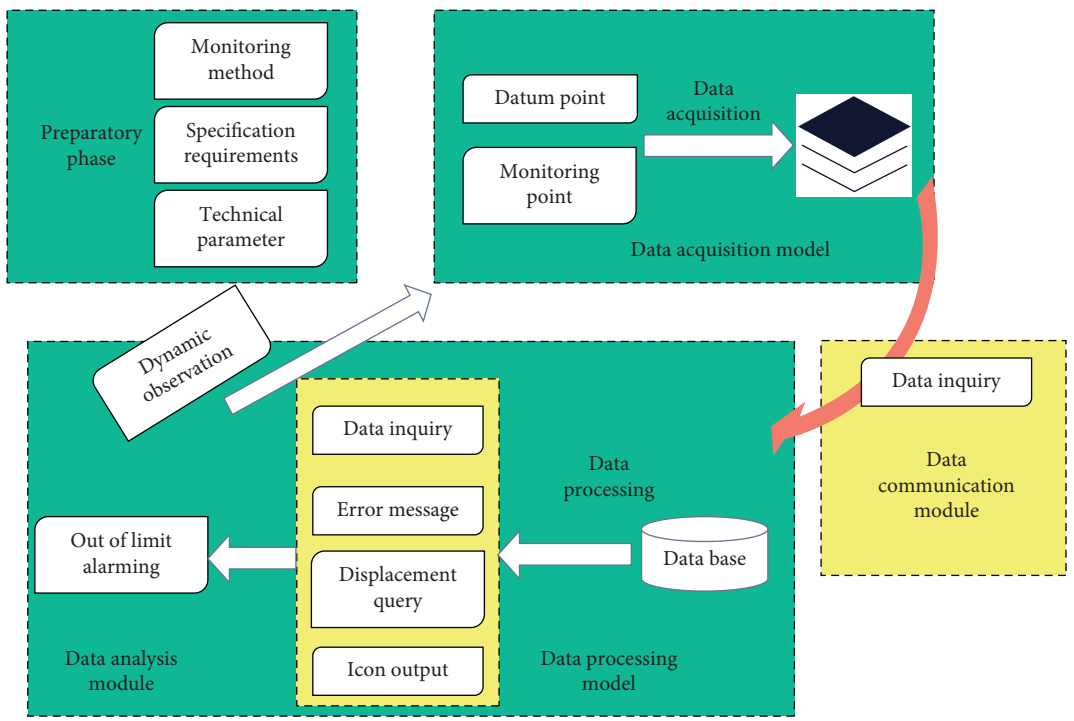

Figure 7: Structure diagram of robot monitoring system.

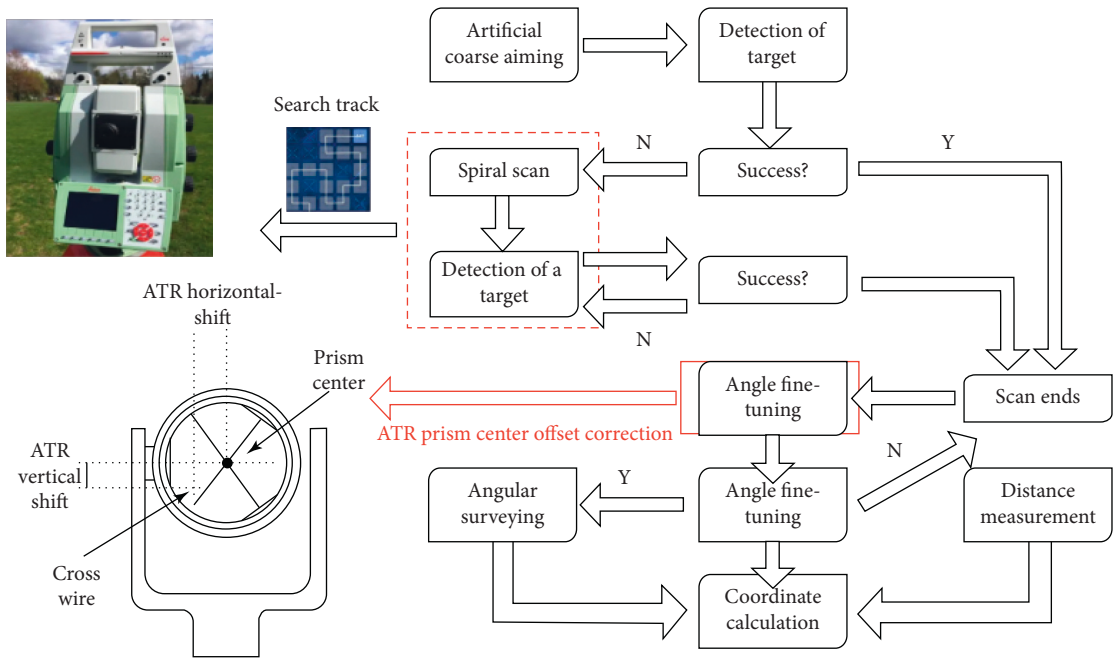

Figure 8: Workflow diagram of robot intelligent detection.

Table 1: Error table of three-dimensional coordinate components of monitoring points.

Point number	Error in north coordinate (mm)	Error in east coordinate (mm)	Point position error in horizontal direction (mm)	Error in vertical direction (mm)
1	0.1414	0.3535	0.3838	0.1818
2	0.0505	0.1414	0.1515	0.2525
3	0.1515	0.4343	0.4646	0.3333
4	0.1414	0.2929	0.3232	0.3636
5	0.303	0.202	0.3636	0.3636
6	0.3232	0.1313	0.3535	0.4444
7	0.2828	0.4646	0.5454	0.2222
8	0.2323	0.3939	0.4545	0.3636
9	0.1616	0.3636	0.3939	0.4141
10	0.3434	0.2525	0.4242	0.3434
11	0.101	0.3232	0.3434	0.2424
12	0.1111	0.4444	0.4545	0.3838
13	0.1313	0.303	0.3333	0.2222
14	0.0505	0.2222	0.2323	0.3535
15	0.2828	0.2727	0.3939	0.2727
16	0.0505	0.2727	0.2727	0.1616

the error table of the three-dimensional coordinate components of the monitoring point is shown in Table 1.

From the above monitoring test results, it can be seen that the engineering safety management system based on robot intelligent detection proposed in this paper has a good effect and can effectively improve the effect of engineering safety management.

4. Conclusion

At present, engineering incidents caused by natural disasters and improper construction are common, making engineering safety early warning and monitoring methods an urgent need of the society. As the relationship between monitored and measured objects becomes more and more complex, people have higher and higher requirements for the timeliness of monitoring data collection and processing and for monitoring data information sharing. Traditional monitoring work is labor-intensive and completed by manual monitoring. There are problems such as irregular data collection, untimely data collection, human error, high personnel investment, high monitoring cost, and high safety production risk. Therefore, the traditional monitoring industry is increasingly unable to meet the requirements of the information age, and transformation is an inevitable trend. This paper combines intelligent monitoring technology to build a monitoring robot system to improve the effect of engineering safety management. It can be seen from the simulation monitoring test results that the engineering safety management system based on robot intelligent

detection proposed in this paper has good effects and can effectively improve the effect of engineering safety management.

Data Availability

The labeled dataset used to support the findings of this study is available from the uthor upon request.

Conflicts of Interest

The author declares no conflicts of interest.

Acknowledgments

This work was supported by Henan Technical College of Construction.

References

[1] Y. Liu, M. Cong, D. Liu, and F. Zhu, "Trajectory planning for porcine abdomen cutting based on an improved genetic algorithm and machine vision for industrial robot," *Robot*, vol. 39, no. 3, pp. 377–384, 2017.

[2] Y. Chen, K. Feng, J. Lu, and Z. Hu, "Machine vision on the positioning accuracy evaluation of poultry viscera in the automatic evisceration robot system," *International Journal of Food Properties*, vol. 24, no. 1, pp. 933–943, 2021.

[3] A. I. Martyshkin, "Motion planning algorithm for a mobile robot with a smart machine vision system," *Nexo Revista Científica*, vol. 33, no. 02, pp. 651–671, 2020.

[4] A. Chaudhury, C. Ward, A. Talasaz et al., "Machine vision system for 3D plant phenotyping," *IEEE/ACM Transactions on Computational Biology and Bioinformatics*, vol. 16, no. 6, pp. 2009–2022, 2019.

[5] D. Wang, H. Song, and D. He, "Research advance on vision system of apple picking robot," *Transactions of the Chinese Society of Agricultural Engineering*, vol. 33, no. 10, pp. 59–69, 2017.

[6] L. Cheng, B. Song, Y. Dai, H. Wu, and Y. Chen, "Mobile robot indoor dual Kalman filter localisation based on inertial measurement and stereo vision," *CAAI Transactions on Intelligence Technology*, vol. 2, no. 4, pp. 173–181, 2019.

[7] V. N. Ganesh, S. G. Acharya, S. Bhat, and S. V. Yashas, "Machine vision robot with real time sensing," *Journal of Advancements in Robotics*, vol. 1, no. 3, pp. 30–34, 2020.

[8] H. Zhang, M. Li, S. Ma, H. Jiang, and H. Wang, "Recent advances on robot visual servo control methods," *Recent Patents on Mechanical Engineering*, vol. 14, no. 3, pp. 298–312, 2021.

[9] S. Smys and G. Ranganathan, "Robot assisted sensing control and manufacture in automobile industry," *Journal of ISMAC*, vol. 01, no. 03, pp. 180–187, 2019.

[10] S. Papanastasiou, N. Kousi, P. Karagiannis et al., "Towards seamless human robot collaboration: integrating multimodal interaction," *International Journal of Advanced Manufacturing Technology*, vol. 105, no. 9, pp. 3881–3897, 2019.

[11] J. Li, J. Yin, and L. Deng, "A robot vision navigation method using deep learning in edge computing environment," *EURASIP Journal on Applied Signal Processing*, vol. 2021, no. 1, p. 22, 2021.

[12] Y. Onishi, T. Yoshida, H. Kurita, T. Fukao, H. Arihara, and A. Iwai, "An automated fruit harvesting robot by using deep learning," *Robomech Journal*, vol. 6, no. 1, p. 13, 2019.

[13] Y. Xiong, Y. Ge, L. Grimstad, and P. J. From, "An autonomous strawberry-harvesting robot: design, development, integration, and field evaluation," *Journal of Field Robotics*, vol. 37, no. 2, pp. 202–224, 2020.

[14] Y. Wang, "On theoretical foundations of human and robot vision," *Learning*, vol. 4, no. 1, pp. 61–86, 2013.

[15] Y. Cho, J. Jeong, and A. Kim, "Model-assisted multiband fusion for single image enhancement and applications to robot vision," *IEEE Robotics and Automation Letters*, vol. 3, no. 4, p. 1, 2018.

[16] A. Tabb and K. M. Ahmad Yousef, "Solving the robot-world hand-eye (s) calibration problem with iterative methods," *Machine Vision and Applications*, vol. 28, no. 5-6, pp. 569–590, 2017.

[17] M. M. A. Al-Isawi and J. Z. Sasiadek, "Guidance and control of a robot capturing an uncooperative space target," *Journal of Intelligent and Robotic Systems*, vol. 93, no. 3-4, pp. 713–721, 2019.

[18] S. Ali, Y. Jonmohamadi, Y. Takeda, J. Roberts, R. Crawford, and A. K. Pandey, "Supervised scene illumination control in stereo arthroscopes for robot assisted minimally invasive surgery," *IEEE Sensors Journal*, vol. 21, no. 10, pp. 11577–11587, 2021.

[19] X. Xu, "Research on teaching reform of mechanical and electronic specialty based on robot education," *OALib*, vol. 08, no. 08, pp. 1–9, 2021.

[20] A. Ghorbandaei Pour, A. Taheri, M. Alemi, and A. Meghdari, "Human–robot facial expression reciprocal interaction platform: case studies on children with autism," *International Journal of Social Robotics*, vol. 10, no. 2, pp. 179–198, 2018.